Prediction of sound reflection by corrugated porous surfaces

J.-F. Allard, O. Dazel,[a] G. Gautier, and J.-P. Groby
Laboratoire d'Acoustique de Université du Maine–CNRS, Avenue Olivier Messiaen, 72085 Le Mans, France

W. Lauriks
Laboratorium voor Akoestishe and Thermal Physics, Katholieke Universiteit Leuven, Heverlee, B-3001 Belgium

(Received 22 July 2010; revised 3 January 2011; accepted 5 January 2010)

The coupled mode (CM) and finite-element methods (FEMs) are developed and used to predict the acoustic reflection coefficient of a semi-infinite porous medium with closely spaced two-dimensional (2D) periodical corrugations. These methods are also applied to predict the reflection coefficient of a periodic array of porous corrugations installed on an acoustically rigid surface. It is shown that the predictions by the both methods agree closely. The reflection coefficient and Brewster angle of total refraction for the corrugated semi-infinite medium predicted with these methods are compared against that predicted by the Biot/Tolstoy/Howe/Twersky and extended Twersky models. A similar analysis is carried out for porous corrugations set on a rigid backing. The behavior of the reflection coefficient and the pole in the expression for the reflection coefficient located close to grazing incidence is studied. © *2011 Acoustical Society of America*. [DOI: 10.1121/1.3552870]

PACS number(s): 43.20.Gp, 43.20.Jr, 43.55.Ev [KVH] Pages: 1696–1706

I. INTRODUCTION

Sound reflection by corrugated porous media has been previously studied by Attenborough and Taherzadeh[1] who proposed a heuristic extension of the Biot/Tolstoy[2] model by using a previous model by Lucas and Twersky[3] [Biot/Tolstoy/Howe/Twersky (BTHT)]. In a more recent work, Boulanger *et al.*[4] presented a version of Twersky's theory[5] extended to porous corrugated media, the extended Twersky (ET) model.

In both initial models, the reflecting surface is a plane with corrugations. The plane is rigid and impervious in the Twersky model[5] and of the same nature as the corrugations in the Tolstoy model.[2] The fluid medium is replaced by an equivalent rigid framed porous medium in the BTHT and the ET models. Both initial models assume that the height of the corrugations is much smaller than the wavelength in the upper medium, and for a periodic distribution of corrugations, the distance D between corrugations is smaller than the wavelength. Only one mode propagates. The ratio of the reflected and the incident propagating mode can be predicted from the surface admittance and the related reflection coefficient with the Twersky model, but the admittance does not appear explicitly in the Tolstoy model, except when the underlying plane is rigid and impervious. The BTHT model provides a surface admittance related to the Tolstoy model, and the ET model generalizes the Twersky model for the case of a porous underlying plane. The extensions correspond to simple choices which give predictions identical to the initial models for an impervious and rigid underlying plane, at grazing incidence for the BTHT model and at all angles of incidence for the ET model.

Indirect measurements close to grazing incidence of the surface admittance have been obtained for a semi-infinite sand layer with regularly spaced corrugations. Predictions with the BTHT and the ET methods are in a reasonable agreement with measurements, but these comparisons do not provide precise information concerning the validity of the methods in a large range of angles of incidence.

Using an equivalent fluid medium, the finite-element method (FEM) has been used by Easwaran and Munjal[6] and the boundary-condition-transfer algorithm was considered by Kar and Munjal[7] to predict sound absorption by wedges at normal incidence. In the context of the Biot theory, the FEM has been used by Kang and Bolton[8] and by Schneider.[9] The double porosity theory by Olny and Boutin[10] has been used by Bécot *et al.*[11] to predict the sound absorption coefficient of a wedge at normal plane-wave incidence.

A new method of predicting the reflection coefficient of two-dimensional (2D) corrugated porous media at oblique incidence and for inhomogeneous waves is worked out. This method is inspired by a method developed by Evans[12] which deals with the problem of propagation in an isovelocity water column, including depth variation and a penetrable bottom. A similar method has also been used to model sound propagation in ducts with variable cross-section by Pagneux *et al.*[13] With the new method, there is no limitation concerning the height of the corrugations and the distance between the corrugations. If the distance D is larger than the wavelength and several modes propagate, the ratios of the different amplitudes can be predicted. Different approximations are used as indicated in Sec. III. Comparisons are performed with the results obtained with a 2D FEM to validate the new method in a large range of angles of incidence. When D is smaller than the wavelength, a reflection coefficient can be calculated with the ratio of the reflected and the incident propagating mode and comparisons can be performed with the BTHT and the ET models. Comparisons are also performed for the Brewster angle of the semi-infinite layer with corrugations and for the pole of the reflection coefficient close to grazing incidence for the impervious backing with corrugations. The chosen time dependence is $e^{-i\omega t}$ with

[a]Author to whom correspondence should be addressed. Electronic mail: olivier.dazel@univ-lemans.fr

 0001-4966/2011/129(4)/1696/11/$30.00

$i=\sqrt{-1}$. $\Re()$ and $\Im()$ are, respectively, the real and imaginary part functions of complex numbers.

II. THE DIFFERENT MODELS

A. Porous medium

Equivalent fluids are considered in this paper. The model by Johnson *et al.*[14] is used for the effective density ρ_1 and the model by Champoux and Allard[15] for the bulk modulus χ_1. These two quantities are associated with the homogenized medium. The following expressions[16] are used for ρ_1 and χ_1 at circular frequency ω:

$$\rho_1=\frac{\rho_0}{\phi}\left(\alpha_\infty-\frac{\nu}{i\omega q_0}\sqrt{1-\left(\frac{2\alpha_\infty q_0}{\phi\Lambda}\right)^2\frac{i\omega}{\nu}}\right), \tag{1}$$

$$\chi_1=\frac{\gamma P_0/\phi}{\gamma-(\gamma-1)\left(1-\frac{\nu\prime}{i\omega q_0}\sqrt{1-\left(\frac{2\alpha_\infty q_0}{\phi\Lambda\prime}\right)^2\frac{i\omega}{\nu\prime}}\right)^{-1}}. \tag{2}$$

In these equations, ν is the kinematic viscosity ($\nu=\eta/\rho_0$), where η is the air dynamic viscosity and ρ_0 is the air density. $\nu'=\nu/\mathrm{Pr}$, where Pr is the Prandtl number. q_0 is the viscous permeability ($q_0=\eta/\sigma$), where σ is the static flow resistivity, α_∞ is the tortuosity, ϕ is the porosity, Λ is the viscous characteristic dimension, and Λ' is the thermal characteristic dimension. The ratio of the specific heats is denoted by γ. P_0 represents the static atmospheric pressure. A factor ϕ is set at the denominator of Eqs. (5.34) and (5.36) of Ref. 16 because the equivalent fluid is related to the whole porous medium (see Secs. V–VII in Ref. 16). The porous medium is then represented by the equivalent displacement $u_{\mathrm{eq}}=\phi u_f$ (where u_f is the displacement of fluid in the pores) which is associated with the total displacement to ensure simple continuity relations.[17] Both the normal displacement and the pressure are continuous at the interface between air and the porous medium. Constitutive law and motion equation are given by

$$-p=\chi_1\nabla.u_{\mathrm{eq}},\quad -\omega^2\rho_1 u_{\mathrm{eq}}=-\nabla p. \tag{3}$$

B. BTHT model

The specular reflection is modeled in terms of the surface impedance. Only the case of a regular spacing is considered in the present work. The corrugations and the underlying plane are of the same nature in the Tolstoy model, but they can differ in the BTHT model. The normalized surface admittance $\beta^*=Z_0/Z_s$, where Z_0 is the characteristic impedance of air and Z_s is the surface impedance of the corrugated porous medium, is given by[1]

$$\beta^*=-ik_0^2\varepsilon_{01}^*\cos^2(\varphi)+\beta, \tag{4}$$

where φ is the angle between the corrugations and the incidence plane. k_0 is the wave-number in air, β is the normalized surface admittance of the porous surface without corrugations, and ϵ_{01}^* is given by

$$\varepsilon_{01}^*=a_{01}^*-b_{01}^*, \tag{5}$$

with

$$a_{01}^*=2V\frac{\rho_1-\rho_0}{\rho_1+\rho_0}.\frac{s_{2\mathrm{D}}}{v_{2\mathrm{D}}} \tag{6}$$

and

$$b_{01}^*=V(1-\chi_0/\chi_1). \tag{7}$$

χ_0 and χ_1 are the bulk moduli of the air and the porous medium, respectively, and V is the raised cross-sectional area per unit length. In the case of hemi-circular corrugations of radius r with a distance D between corrugations, $V=\frac{\pi r^2}{2D}$. In addition, one has

$$s_{2\mathrm{D}}=\frac{\rho_0+\rho_1}{2(\rho_1+K\rho_0)}(1+K), \tag{8a}$$

$$v_{2\mathrm{D}}=1+\frac{2\pi V}{3D}\frac{\rho_1-\rho_0}{\rho_1+\rho_0}s_{2\mathrm{D}}. \tag{8b}$$

K is a hydrodynamic shape factor equal to 1 for semi-cylindrical cylinders.[18]

In the initial Tolstoy's model, the acoustic potential in the overlying fluid is the sum of a smooth boundary solution Φ_0 (reflection by the plane without corrugations) plus a perturbation Φ_s due to the roughness. The potentials Φ_0 and Φ_s are related by [see Eq. (3.68) in Ref. 2 where a superscript 2 is omitted]

$$\frac{\partial\Phi_s}{\partial z}=-\varepsilon_{12}^*\left(\kappa^2\cos^2(\varphi)-\frac{b_{01}}{\varepsilon_{12}^*}\gamma^2\right)(\Phi_0+\Phi_s), \tag{9}$$

where κ is the horizontal wave-number and γ is the z-wave-number in the overlying fluid. If the underlying plane is rigid and impervious, Eqs. (9) and (4) are identical at grazing incidence, but they are very different close to normal incidence.

C. ET model

A presentation of the model was given by Boulanger *et al.*[4] for semi-circular porous cylindrical corrugations on a hard impervious backing. For regularly spaced cylinders, the normalized admittance is given by

$$\beta_{2\mathrm{D}}=\beta-ik_0V\left[\left(\frac{\chi_0}{\chi_1}-1\right)-\frac{B-1}{1+(B-1)A_2}\sin^2(\theta)\right], \tag{10}$$

$$A_2=\frac{1}{2}-\frac{I_2\pi r^2}{4\pi D^2},\quad I_2=\frac{(\pi r^2)}{3D^2}, \tag{11}$$

$$B=\frac{\rho_0}{\rho_1}. \tag{12}$$

III. COUPLED MODE (CM) MODEL

The model only concerns even corrugations, i.e., those associated to symmetrical corrugations. A spatial period of the porous surface is represented in Fig. 1. The origin of the x axis is at the middle of the period. Under the corrugation,

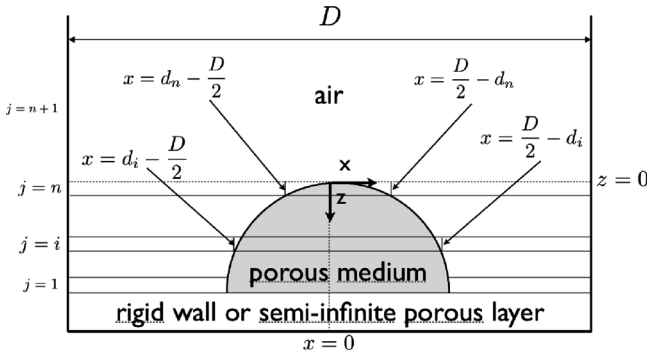

FIG. 1. Configuration of the problem.

there is a layer of porous medium which can be infinite [corrugations over a semi-infinite layer (half space)], finite, or equal to 0 for corrugations on a rigid impervious surface. The corrugation is replaced by a superposition of n elementary volumes separated by horizontal plane surfaces, where the limits between the porous medium and the air are vertical plane surfaces. The elementary volumes are numbered with j. For $j=1$, the elementary volume material is the porous medium, and for $j>1$, volumes are subdivided into three sub-volumes, one with porous medium (for $|x|<D/2-d_j$, where d_j is the length of the air sub-volume) and two with air. The geometrical difference between two adjacent elementary volumes should be limited otherwise a large number of modes are needed to satisfy the continuity of pressure and z velocity component. Hence, the increase of the length d_j is constant from $j=1$ to $j=n$ and $d_j=(j-1)D/(2n)$. Let e_j be the thickness of layer j. e_j can be equal to zero for elementary volumes called "virtual" elementary volumes. These volumes are added in the case of strong discontinuities to avoid numerical drawbacks. The different corrugation shapes are related to different dependences of e_j on j.

An incident plane or inhomogeneous wave with a k_x wave-number x-component creates in air for $z<0$ the refracted modes (Bloch waves) with x-wave-numbers $k_{x,n+1,l}$ given by

$$k_{x,n+1,l}=k_x+\frac{2\pi l}{D},\quad l\in[-2L;2L]_{\mathbb{N}}. \tag{13}$$

In the calculations, the number of the refracted modes is finite, and the truncation is controlled by integer N so that $|l|<N$. The subscript $n+1$ is used, because the air at $z<0$ is above the elementary volume n. The related z-wave-number vector components are given by

$$k^{\pm}_{z,n+1,l}=\pm\sqrt{k_0^2-k^2_{x,n+1,l}}. \tag{14}$$

The spatial dependence of a mode above the corrugations is $\exp(i(k_{x,n+1,l}x+k^{\pm}_{z,n+1,l}z))$. The pressure presents $2N+1$ different dependencies on x, and $4N+2$ modes are retained. If k_x is real, then $k^{+}_{z,n+1,0}$ is related to the incident wave and $k^{-}_{z,n+1,0}$ is related to the specular reflected wave. For $l\neq 0$, with the convention $\Im(k^{+}_{z,n+1,l})>0$, $k^{+}_{z,n+1,l}$ corresponds to an unphysical mode which increases when $z\to-\infty$. $k^{-}_{z,n+1,l}$ corresponds to a physical mode. For $j=1$ in the lower elementary volume, and above in the case of a semi-infinite layer, the x-wave-numbers $k_{x,1,l}$ are equal to $k_{x,n+1,l}$ and the z-wave-number vector components are given by

$$k^{\pm}_{z,1,l}=\pm\sqrt{k_1^2-k^2_{x,1,l}}. \tag{15}$$

The acoustic field in the elementary volume j is approximated by a superposition of $4N+2$ modes. These modes correspond to $2N+1$ x-dependencies and are related to two opposite z-wave-number vector component $\pm k_{z,j,l}$. These z wave-numbers are common for the three sub-volumes. Therefore, a mode can propagate vertically in an elementary volume as a plane-wave.

For layer j and wave l, mode $p_{j,l}$ is defined as the solution of the problem

$$\mathcal{L}_j p_{j,l}=-\alpha^2_{j,l}p_{j,l}, \tag{16}$$

with $\mathcal{L}_j$ a differential operator defined by

$$\mathcal{L}_j=-\frac{d^2}{dx^2}+(k_0^2-k_j^2(x))\quad\text{with}\quad k_j^2(x)=\omega^2\frac{\rho_j(x)}{\chi_j(x)}. \tag{17}$$

Density $\rho_j(x)$ [respectively, compressibility $\chi_j(x)$] is equal to ρ_0 (respectively, χ_0) in sub-volumes 1 and 3 and equal to ρ_1 (respectively, χ_1) in sub-volume 2. Let $\alpha_{j,l}$ and $\beta_{j,l}$ be the x-wave-number components in the air sub-volumes and in the porous sub-volume, respectively. The x-dependences of mode $p_{j,l}$ can be written in the form

$$p_{j,l}(x)=A_{1,j,l}\exp(-i\alpha_{j,l}x)+B_{1,j,l}\exp(i\alpha_{j,l}x),\quad D/2\geq x\geq D/2-d_j, \tag{18a}$$

$$p_{j,l}(x)=A_{3,j,l}\exp(-i\alpha_{j,l}x)+B_{3,j,l}\exp(i\alpha_{j,l}x),\quad D/2\geq -x\geq D/2-d_j, \tag{18b}$$

$$p_{j,l}(x)=A_{2,j,l}\exp(-i\beta_{j,l}x)+B_{2,j,l}\exp(i\beta_{j,l}x),\ |x|\geq d_j. \tag{18c}$$

The following conditions should also be satisfied:

(1) Periodicity condition for pressure $p_{j,l}$ and x-velocity component v_x (Floquet theorem)

$$p_{j,l}(x=D/2)=p_{j,l}(x=-D/2)\delta,\qquad v_{j,l}(x=D/2)=v_{j,l}(x=-D/2)\delta, \tag{19}$$

with

$$\delta=e^{ik_xD}. \tag{20}$$

(2) Common z-wave-number vector component for the three sub-volumes

$$k_0^2-\alpha^2_{j,l}=k_1^2-\beta^2_{j,l}. \tag{21}$$

(3) Pressure continuity and x-velocity component continuity at the boundaries between adjacent sub-volumes.

All these conditions lead to the following dispersion relation:

$$w(\alpha_{j,l},\beta_{j,l})=0, \tag{22}$$

$$w(\alpha,\beta) = 4\cos(k_x D) - \cos(\beta(D-2d_j)+2\alpha d_j)\left(1+\frac{\alpha\rho_1}{\beta\rho_0}\right) \times \left(1+\frac{\beta\rho_0}{\alpha\rho_1}\right) + \cos(\beta(D-2d_j)-2\alpha d_j) \times \left(1-\frac{\alpha\rho_1}{\beta\rho_0}\right)\left(1-\frac{\beta\rho_0}{\alpha\rho_1}\right)$$

For $k_x = 0$, this dispersion relation reduces to

$$\frac{\alpha_{j,l}}{\rho_0}\cos(\beta_{j,l}(d_j - D/2))\sin(\alpha_{j,l}D) = \frac{\beta_{j,l}}{\rho_1}\sin(\beta_{j,l}(d_j - D/2))\cos(\alpha_{j,l}D), \quad (23)$$

which is the dispersion relation at normal incidence. The latter can be obtained by simpler calculations. The details of the calculations to obtain Eq. (22) are given in Appendix A which includes the equations used to calculate the coefficients A and B in Eq. (18). An iterative method is used to obtain the numerical value of $\beta_{j,l}$ and the other wave-number components $\alpha_{j,l}$ and $k_{z,j,l}$ for the $2N+1$ x-dependences in each volume. The iterative method is described in Appendix C.

The x pressure dependences in any elementary volume are orthogonal. The orthogonality relation can be written as

$$\int_{-D/2}^{D/2} \frac{p_{j,l}(x)p_{j,m}(-x)}{\rho_j(x)}\,dx = 0, \quad l \neq m. \quad (24)$$

This relation generalizes the orthogonality relation at normal incidence in Ref. 12 and the proof is in Appendix B. After normalization by a factor $\gamma_{j,l}$

$$\hat{p}_{j,l} = \frac{p_{j,l}}{\sqrt{\gamma_{j,l}}}, \quad \gamma_{j,l} = \int_{-D/2}^{D/2} \frac{p_{j,l}(x)p_{j,l}(-x)}{\rho(x)}\,dx. \quad (25)$$

The x-dependences satisfy the orthonormalization relation

$$\int_{-D/2}^{D/2} \frac{\hat{p}_{j,l}(x)\hat{p}_{j,m}(-x)}{\rho(x)}\,dx = \delta_{lm}. \quad (26)$$

This equation has been systematically verified numerically in the calculation to check the precision in the evaluation of the parameter A, B, α, and β.

The coupling equations between modes in adjacent elementary volumes are obtained from the equations related to the continuity of pressure and z-velocity components at the interface between the elementary volumes j and $j+1$.

The x-dependence of the total pressure in the elementary volume j and $j+1$ can be written as

$$P_j(x) = \sum_{m=-N}^{N} (C_{j,m}^{+} + C_{j,m}^{-})\hat{p}_{j,m}(x), \quad (27a)$$

$$P_{j+1}(x) = \sum_{l=-N}^{N} (C_{j+1,l}^{+} + C_{j+1,l}^{-})\hat{p}_{j,l}(x). \quad (27b)$$

$C_{j,m}^{+}$ is the amplitude of the mode with $k_z = k_{z,j,m}$ and $C_{j,m}^{-}$ is the amplitude of the mode with $k_z = -k_{z,j,m}$ at the interface. Pressure and velocity continuity equations at the interface can be written as

$$\sum_{m=-N}^{N} (C_{j,m}^{+} + C_{j,m}^{-})\hat{p}_{j,m}(x) = \sum_{l=-N}^{N} (C_{j+1,l}^{+} + C_{j+1,l}^{-})\hat{p}_{j,m}(x), \quad (28a)$$

$$\sum_{m=-N}^{N} \frac{k_{z,m}^{j}(C_{j,m}^{+} - C_{j,m}^{-})\hat{p}_{j,m}(x)}{\rho_j(x)} = \sum_{l=-N}^{N} \frac{k_{z,l}^{j+1}(C_{j+1,l}^{+} - C_{j+1,l}^{-})\hat{p}_{j+1,l}(x)}{\rho_{j+1}(x)}. \quad (28b)$$

Using the orthogonality relations, Eqs. (28) lead to

$$C_{j+1,l}^{+} = \frac{1}{2}\sum_{m=-N}^{N}\left[D_{RL}(j,m,j+1,l) + D_{LR}(j,m,j+1,l)\frac{k_{z,m}^{j}}{k_{z,m}^{j+1}}\right]C_{j,m}^{+} + \frac{1}{2}\sum_{m=-N}^{N}\left[D_{RL}(j,m,j+1,l) - D_{LR}(j,m,j+1,l)\frac{k_{z,m}^{j}}{k_{z,m}^{j+1}}\right]C_{j,m}^{-}, \quad (29)$$

$$C_{j+1,l}^{-} = \frac{1}{2}\sum_{m=-N}^{N}\left[D_{RL}(j,m,j+1,l) - D_{LR}(j,m,j+1,l)\frac{k_{z,m}^{j}}{k_{z,m}^{j+1}}\right]C_{j,m}^{+} + \frac{1}{2}\sum_{m=-N}^{N}\left[D_{RL}(j,m,j+1,l) + D_{LR}(j,m,j+1,l)\frac{k_{z,m}^{j}}{k_{z,m}^{j+1}}\right]C_{j,m}^{-}. \quad (30)$$

D_{LR} and D_{RL} are defined by

$$D_{LR}(j,m,j+1,l) = \int_{0}^{D/2} \frac{\hat{p}_{j,m}(x)\hat{p}_{j+1,l}(-x)}{\rho_j(x)}\,dx, \quad (31a)$$

$$D_{RL}(j,m,j+1,l) = \int_{0}^{D/2} \frac{\hat{p}_{j,m}(x)\hat{p}_{j+1,l}(-x)}{\rho_{j+1}(x)}\,dx. \quad (31b)$$

The amplitudes of the modes at the lower face of the elementary volume $j+1$ are modified by the propagation in the z direction on a length equal to the thickness e_{j+1} of the elementary volume. The coefficients $C_{j+1,l}^{\pm}$ must be multiplied by $\exp(\pm ik_{z,j+1,l}e_{j+1})$, the axis z being directed toward the rigid-backing. For each interface between two elementary volumes, a $(4N+2)\times(4N+2)$ transfer matrix $[M_{j+1,j}]$ links amplitudes in the elementary volume j at the interface j, $j+1$ to amplitudes in the elementary volume

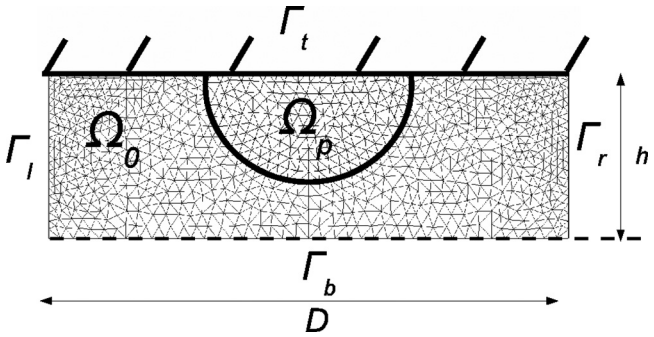

FIG. 2. Configuration of the FEM problem.

$j+1$ at the interface $j+1$, $j+2$. The product $[M_t] = [M_{n+1,n}][M_{n,n-1,j}] \cdots [M_{2,1}]$ links the amplitudes in the elementary volume 1 at the interface with the elementary volume 2 to the amplitudes in air at $z=0$.

There are two approximations in this model. Only a finite number of modes is used, and the geometry of the original corrugation is different from the one of the stack of elementary volumes.

IV. FINITE-ELEMENT MODELING

The problem is presented in Fig. 2. A rectangular domain Ω of length D and thickness h is considered. It should be noted that a different coordinate system is defined in this section compared to the previous one as a sake of simplification. Here, the origin of the system is at the bottom-left corner. Ω is subdivided in two subdomains: Ω_p (respectively, Ω_0) corresponds to the porous material (respectively, air). The porous material is modeled by an equivalent fluid model so that the propagation equation on the whole Ω domain can be written in the following form:

$$\frac{1}{\omega^2\rho(\mathbf{x})}\nabla^2 p + \frac{p}{\chi(\mathbf{x})} = 0. \tag{32}$$

$\rho(\mathrm{x})$ is equal to ρ_0 in Ω_0 and to ρ_1 in Ω_p. $\chi(x)$ is equal to χ_0 in Ω_0 and to χ_1 in Ω_p. The boundary of the Ω domain, denoted by Γ, is divided into four interfaces as depicted in Fig. 2. Γ_t corresponds to a rigid wall so that the normal displacement is equal to zero. Γ_l and Γ_r correspond to the periodicity interfaces so that both displacement and pressure should satisfy the Floquet theorem (19). Γ_b is the interface with a semi-infinite air layer. On this boundary, both pressure and normal displacement can be expressed as a function of the amplitude of the incident and reflected waves

$$p_{|\Gamma_b}(x) = e^{ik_x x} + \sum_{l\in\mathbb{Z}} R^l\, e^{ik_{x,n+1,l}x}, \tag{33}$$

$$u_{n|\Gamma_b}(x) = -\frac{i}{\rho_0\omega^2}\left(\sum_{l\in\mathbb{Z}} -k_{z,n+1,l}R^l\, e^{ik_{x,n+1,l}x} + k_{z,n+1,0}\, e^{ik_x x}\right). \tag{34}$$

The incident wave is assumed to have unity amplitude so that R^l are the reflection coefficients of the plane waves denoted by superscript l. These coefficients are the unknowns of the problem.

The variational formulation of the problem reads

$$\forall q \in H^1(\Omega) \int_\Omega \frac{\nabla p\, \nabla q}{\omega^2\rho(\mathbf{x})} - \frac{pq}{\chi(\mathbf{x})}\,\mathrm{d}\Omega = \oint_\Gamma u_n q\,\mathrm{d}S, \tag{35}$$

with $H^1(\Omega)$ is the Sobolev space associated with Ω.

Ω is discretized by a Delaunay triangulation with the $\Omega_p - \Omega_0$ interface as the internal boundary. This results in the density $\rho(\mathrm{x})$ and compressibility $K(\mathrm{x})$ being constant on each triangle of the mesh. The boundary term can be rewritten as

$$\begin{aligned}\oint_\Gamma u_n q\,\mathrm{d}S = &-\frac{i}{\rho_0\omega^2}\oint_{\Gamma_b} \\ &\times\left(\sum_{l\in\mathbb{Z}} k_{z,n+1,l}R^l\, e^{ik_{x,n+1,l}x} + k_{z,n+1,0}\, e^{ik_x x}\right) q\,\mathrm{d}S \\ &+\oint_{\Gamma_l} u_n q\,\mathrm{d}S + \delta\oint_{\Gamma_l} u_n q\,\mathrm{d}S.\end{aligned} \tag{36}$$

The pressure is approximated by a quadratic finite-element, thereby leading to a discretized problem of n_e elements and n nodes. To ensure the periodicity, this mesh also has similar n_l nodes on Γ_l and Γ_r. Let n_b be the number of nodes on Γ_b. The finite-element system is of the following form

$$\left(\frac{[\widetilde{\mathbf{H}}]}{\omega^2} - [\widetilde{\mathbf{Q}}]\right)\mathbf{P} = \mathbf{u}_n. \tag{37}$$

P is the unknown vector of the n pressures at the nodes. $[\widetilde{\mathbf{H}}]$ and $[\widetilde{\mathbf{Q}}]$ represent the kinetic and compression energy matrices

$$[\widetilde{\mathbf{H}}] = \sum_{i_e=1}^{n_e}\int_{\Omega_e} \frac{[\mathbf{L}_e]^t[\nabla\mathbf{N}_e]^t[\nabla\mathbf{N}_e][\mathbf{L}_e]}{\rho_e}\mathrm{d}\Omega, \tag{38}$$

$$[\widetilde{\mathbf{Q}}] = \sum_{i_e=1}^{n_e}\int_{\Omega_e} \frac{[\mathbf{L}_e]^t[\mathbf{N}_e]^t[\mathbf{N}_e][\mathbf{L}_e]}{\chi_e}\mathrm{d}\Omega. \tag{39}$$

$[\mathrm{N}_e(\mathrm{x})]$ is the 1×6 matrix of the shape function on Ω_e. $[\mathrm{L}e]$ is a $n_e \times n$ matrix element e used for the correspondence between the local and global degrees of freedom. ρ_e and χ_e represent, respectively, the values of $\rho(\mathrm{x})$ and $\chi(\mathrm{x})$ on element e. $\mathrm{u_n}$ is the discretized vector of the displacement at the boundary. Its values are null on Γ_t, verifying the periodicity relations on Γ_l and Γ_r. In order to model the continuity of displacement and pressure on Γ_b, sums (33) and (34) are truncated to the first n_b terms (order: 0, 1, −1, 2,....). The corresponding n_b reflection coefficients are merged in the R vector, which is an unknown of the problem. Note that this number of reflected waves is not equal to N of the CM method. n_b additional equations are then added, associated with the pressure continuity relations (33). The displacement continuity relations are formally written so that the displacements are expressed as a function of R and system (37) is transformed to

$$\begin{bmatrix} \frac{\widetilde{[\mathbf{H}]}}{\omega^2} - [\widetilde{\mathbf{Q}}] & [\mathbf{S}] \\ [\mathbf{T}] & [\mathbf{U}] \end{bmatrix} \begin{Bmatrix} \mathbf{P} \\ \mathbf{R} \end{Bmatrix} = \begin{Bmatrix} \mathbf{u}_n' \\ \mathbf{P}_b \end{Bmatrix}. \tag{40}$$

Algebraic manipulations are now processed to account for the periodicity and to impose the plane-wave loading on the system. The equations and degrees of freedom of Eq. (40) are first reordered. Let P_l (respectively, P_r and P_i) be the degrees of freedom associated with the left boundary (respectively, right boundary and internal nodes). Let $[\Delta]$ be the orthogonal Boolean correspondence matrix between the original and reordered degrees of freedom

$$\mathbf{P} = [\Delta] \begin{Bmatrix} \mathbf{P}_l \\ \mathbf{P}_i \\ \mathbf{P}_r \end{Bmatrix}, \qquad \begin{Bmatrix} \mathbf{P} \\ \mathbf{R} \end{Bmatrix} = \underbrace{\begin{bmatrix} [\Delta] & [\mathbf{0}] \\ [\mathbf{0}] & [\mathbf{I}_{n_b}] \end{bmatrix}}_{[\Delta']} \begin{Bmatrix} \mathbf{P}_l \\ \mathbf{P}_i \\ \mathbf{P}_r \\ \mathbf{R} \end{Bmatrix}. \tag{41}$$

System (40) is then reordered by pre-multiplication by $[\Delta']^t$ and leads to

$$\begin{bmatrix} [\mathbf{A}] & [\mathbf{B}] & [\mathbf{C}] & [\mathbf{D}] \\ [\mathbf{E}] & [\mathbf{F}] & [\mathbf{G}] & [\mathbf{H}] \\ [\mathbf{I}] & [\mathbf{J}] & [\mathbf{K}] & [\mathbf{L}] \\ [\mathbf{M}] & [\mathbf{N}] & [\mathbf{O}] & [\mathbf{P}] \end{bmatrix} \begin{Bmatrix} \mathbf{P}_l \\ \mathbf{P}_i \\ \mathbf{P}_r \\ \mathbf{R} \end{Bmatrix} = \begin{Bmatrix} \mathbf{u}_l \\ \mathbf{u}_i \\ \mathbf{u}_r \\ \mathbf{P}_b \end{Bmatrix}. \tag{42}$$

The nine matrices of the upper left corner of this problem correspond to the matrix product

$$[\Delta]^t \left[\frac{\widetilde{[\mathbf{H}]}}{\omega^2} - [\widetilde{\mathbf{Q}}] \right] [\Delta] \tag{43}$$

and are split in order to simplify the following algebraic manipulations.

The periodicity induces that $\mathrm{P}_r = \delta \mathrm{P}_l$. In addition, u_l and u_r can be written as

$$\mathbf{u}_l = \mathbf{u}_l' + \mathbf{u}_p, \quad \mathbf{u}_r = \mathbf{u}_r' - \delta\, \mathbf{u}_p. \tag{44}$$

u_p is the displacement at the boundary, which remains an unknown of our problem. It can be eliminated by linear combination of the rows of system (42). Finally, one has

$$\begin{bmatrix} [\mathbf{A}]\delta + [\mathbf{I}] + \delta([\mathbf{C}]\delta + [\mathbf{K}]) & [\mathbf{B}]\delta + [\mathbf{J}] & [\mathbf{D}]\delta + [\mathbf{L}] \\ [\mathbf{E}] + \delta[\mathbf{G}] & [\mathbf{F}] & [\mathbf{H}] \\ [\mathbf{M}] + [\mathbf{O}]\delta & [\mathbf{N}] & [\mathbf{P}] \end{bmatrix} \begin{Bmatrix} \mathbf{P}_l \\ \mathbf{P}_i \\ \mathbf{R} \end{Bmatrix} = \begin{Bmatrix} \mathbf{u}\prime_l + \mathbf{u}\prime_r \\ \mathbf{u}_i \\ \mathbf{P}_b \end{Bmatrix}. \tag{45}$$

The resolution of this system provides the reflection coefficients R of the plane waves. A direct sparse solver is used for the resolution process. The quality of the solution of system has been checked by evaluating the residual associated with the linear system. No major numeric problems occur.

V. ILLUSTRATION

Two configurations have been considered at 1 kHz, a semi-infinite porous layer with semi-circular corrugations of radius $r = 2$ cm separated by a distance $D = 10$ cm and the same corrugations set on an impervious and rigid backing. The parameters that characterize the porous medium are given in Table I. The specular reflection coefficient is predicted with the CM model and FEM. These predictions are compared with the BTHT and the ET models.

With this choice of geometry and frequency, the height r of the corrugations is much smaller than the wavelength and the distance D is smaller than the wavelength. The validity conditions for the BTHT and ET models must be fulfilled. There is only one propagating mode and a reflection coefficient can be evaluated with the CM model using the predicted ratio of the amplitudes of the reflected and the incident propagating mode. This will allow a comparison with the predictions of BTHT and the ET models. With these acoustic parameters, the reduced characteristic impedance in the equivalent fluid is $Z_1 = 1.33 + 1.62i$. There is a noticeable contrast with air but Z_1 is not very large and the ET model must be used instead of the Twersky model for a semi-infinite underlying porous layer of this material.

A. Comparison of CM and FEM

The CM and FEM are first compared. The results are presented for the rigid-backing configuration. The predictions with the CM model are performed with $2N + 1 = 31$ and $n = 380$ elementary volumes. The thickness of the first elementary volumes must be equal to 0 and remain transparent as far as $d_j = 3$ cm, when the porous medium effectively exists for $|x| > d_j$. Therefore, the thickness e_j of the elementary volume j is given by

$$e_j = 0, \quad j \leq 228 \text{ (Virtual elementary volumes)}, \tag{46a}$$

$$e_j = \sqrt{002^2 - (005 - d_j)^2} - e_{j-1}, \quad j \geq 228. \tag{46b}$$

Progressive and retrograde modes exist in the first layer, but one has $\forall\ m$, $C_{1,m}^{+} = C_{1,m}^{-}$ at the contact surface with the backing. Hence, there are only $2N + 1$ unknown amplitudes which can be calculated.

To compare CM and FEM, different meshes are considered for the FEM. All of them should satisfy the similarity of the nodes on Γ_l and Γ_r. All these meshes differ from each other by the size of the elements (triangles) used for the discretization. This size is compared to the wavelength in the porous medium (20.4 cm at 1 kHz), which is lower than that in air. The meshes are characterized by a λ / n criterion where n is the number of elements per wavelength. Figure 3

TABLE I. Parameters for the porous medium.

Flow resistivity σ	Nm^{-4}	12 000
Porosity ϕ	Ø	0.99
Tortuosity α_∞	Ø	1.01
Viscous characteristic dimension Λ	mm	0.1
Thermal characteristic dimension Λ'	mm	0.4

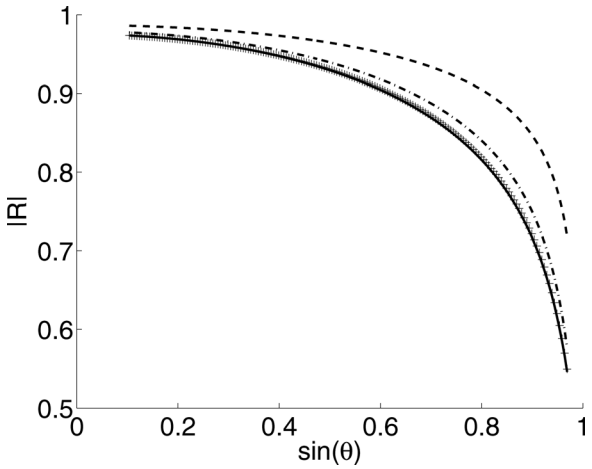

FIG. 3. Specular reflection coefficient versus angle of incidence for different meshes. Solid: CM method; Dashed: $\lambda/2$; Dashed-dotted: $\lambda/4$; '+': $\lambda/10$.

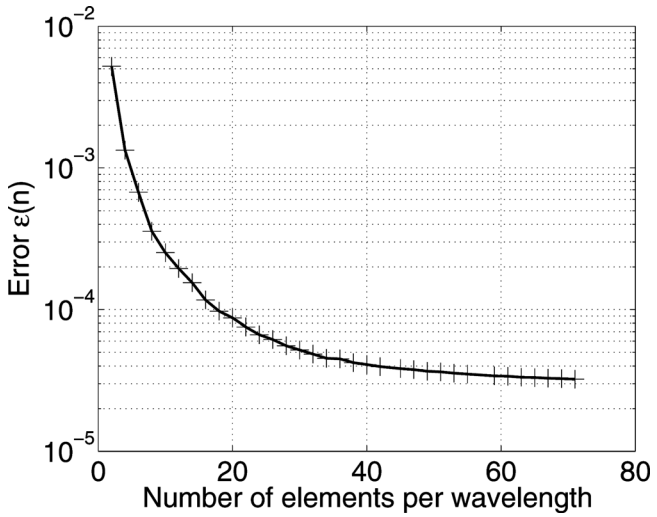

FIG. 4. Evolution of the error $\epsilon(n)$ between CM and FEM versus the discretization size.

presents the modulus of the specular reflection coefficient for $n=2$, 4, 10 discretizations. The convergence can be observed and there is no visual difference between the CM and the $\lambda/10$ FEM result.

In order to check the convergence of the two methods, the error in the Euclidian norm is calculated for each discretization. This error is defined by

$$\varepsilon(n) = \frac{\sum_{i=1}^{n_i} \sqrt{\left|R_{CM}(\sin(\theta_i)) - R_{EF(\lambda/n)}(\sin(\theta_i))\right|^2}}{n_i}, \quad (47)$$

n_i is the number of incident angles. In the present case, $n_i=174$. The angles are chosen so that the sines $\sin(\theta_i)$ are linearly spaced between 0.1 and 0.97. The different models predict a limit equal to 1 when $\sin(\theta)$ tends to 1. In order to get a clear representation of the different predictions with a small vertical scale, the chosen upper limit of $\sin(\theta)$ is 0.97 with a lower limit of 0.1, the implemented version of the CM model cannot be used at normal incidence. R_{CM} $(\sin(\theta_i))$ and $R_{\mathrm{FEN}(\lambda/n)}$ $(\sin(\theta_i))$ are the specular reflection coefficient obtained, respectively, by the CM and FEM for a λ/n discretization. Figure 4 presents the evolution of $\epsilon(n)$ for several discretizations. The asymptotic error is around 3.2×10^{-5}, which indicates that both methods agree for the first four digits. This precision corresponds to a -36 dB error expressed in pressure level. The convergence between CM and FEM has also been verified for a corrugated semi-infinite porous medium. In the following, only results with CM are presented.

B. Comparison between CM, BTHT, and ET models

Comparisons are performed for porous corrugations over a semi-infinite layer of the same porous medium and over a rigid impervious plane. The acoustic parameters for the porous medium and the geometry of the corrugations are indicated at the beginning of the present section. For the semi-infinite medium, the $2N+1$ modes with $\Re(k_{z,1,l})<0$ have an amplitude equal to 0. The amplitude of the $2N$ retrograde modes in air is equal to 0 and the amplitude of the incident wave is arbitrarily taken equal to 1. The matrix $[M_l]$ is used to relate these amplitudes to the $2N+1$ unknown amplitudes in the first elementary volume and to find their values. Knowing all the amplitudes in the first elementary volume, it is possible to evaluate the amplitude of the specular reflected mode. The modulus of the reflection coefficient is shown in Fig. 5 for the corrugated semi-infinite layer and in Fig. 6 for the corrugations over a rigid-backing.

In Fig. 5, predictions of the reflection coefficient modulus obtained by the CM and heuristic methods are shown as a function of the sine of the incident angle θ. Prediction for a single semi-infinite layer without corrugations is also given. The CM and FEM model predictions are represented by only one curve. The admittance of the semi-infinite layer without corrugations is close to that of the BTHT and ET models. This admittance plays a dominant role in Eqs. (4) and (10) for both models. Predictions with the BTHT and ET models have the same order of magnitude as predictions with the

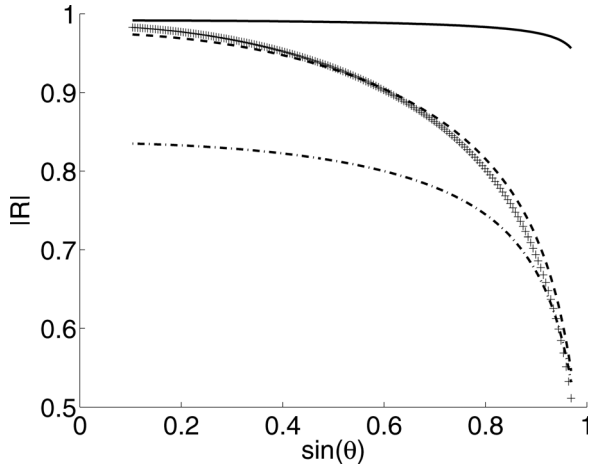

FIG. 5. Reflection coefficient versus incident angle for the corrugated semi-infinite porous medium. Solid: No corrugation; Dashed: CM; Dashed-dotted: BTHT; +: ET.

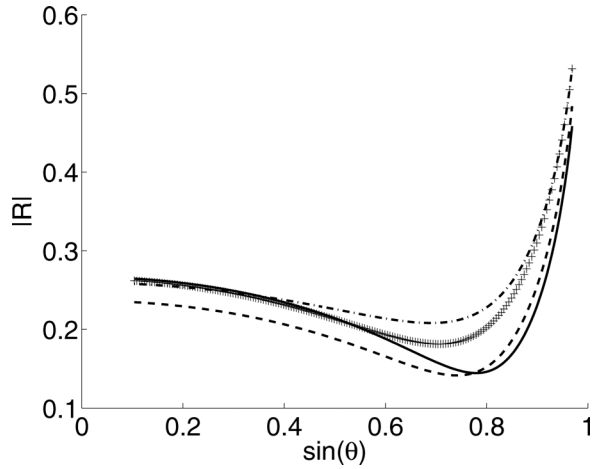

FIG. 6. Reflection coefficient versus incident angle for the corrugated rigid-backing. Solid: Constant thickness layer; Dashed: CM; Dashed-dotted: BTHT; + : ET.

CM model, the largest discrepancies appearing around the minimum of the modulus. The modulus of the reflection coefficient of the semi-infinite layer is not strongly modified by the corrugations at least for the corrugation tested in this work. In Fig. 6, predictions of the reflection coefficient modulus obtained with the CM model and the FEM, the BTHT, and the ET models are presented. The prediction for a layer of constant thickness $l=\pi r^2/(2D)$ having the same volume of porous medium per unit area as the corrugations are also plotted. It appears that the modulus is much smaller with the corrugations than for the layer of constant thickness for all models. The predictions with the ET model and the CM model are very close in the whole range of angles of incidence. With a rigid impervious underlying plane, the ET model is identical to the Twersky model. This shows in this case the validity of the Twersky model. At small angles of incidence, the BTHT model provides a modulus significantly lower than the other models. It was shown in Sec. II that the BTHT model and the initial Tolstoy model are very different close to normal incidence.

As indicated previously, the modulus of the reflection coefficient of the semi-infinite layer is not strongly modified by the corrugations. The modulus for the semi-infinite layer without corrugations is equal to 0 at the Brewster angle θ_b of total refraction[16] which would be real if the medium were lossless. The angle θ_b can be evaluated from pressure measurements close to grazing incidence.[19] It is given by

TABLE II. Brewster angle and modified Brewster angle.

$\sin(\theta_b)$	$0.829 \pm i\,0.128$
$\cos(\theta_b)$	$0.600 - i\,0.176$
$\sin(\theta_{b,\mathrm{CM}})$	$0.801 \pm i\,0.149$
$\cos(\theta_{b,\mathrm{CM}})$	$0.644 - i\,0.185$
$\sin(\theta_{b,\mathrm{BTHT}})$	$0.836 \pm i\,0.227$
$\cos(\theta_{b,\mathrm{BTHT}})$	$0.660 - i\,0.287$
$\sin(\theta_{b,\mathrm{ET}})$	$0.795 \pm i\,0.194$
$\cos(\theta_{b,\mathrm{ET}})$	$0.677 - i\,0.228$

TABLE III. Pole of the reflection coefficient close to $\pi/2$.

$\sin(\theta_p, \mathrm{CL})$	$1.0025 + i\,4.38 \times 10^{-3}$
$\cos(\theta_p, \mathrm{CL})$	$-5.077 \times 10^{-2} + i\,8.625 \times 10^{-2}$
$\sin(\theta_{p,\mathrm{CM}})$	$1.000924 + i\,9.178 \times 10^{-3}$
$\cos(\theta_{p,\mathrm{CM}})$	$-9.136 \times 10^{-2} + i\,0.1006$
$\sin(\theta_{p,\mathrm{BTHT}})$	$1.0027 + i\,9.316 \times 10^{-3}$
$\cos(\theta_{p,\mathrm{BTHT}})$	$-9.044 \times 10^{-2} + i\,0.1031$
$\sin(\theta_{p,\mathrm{ET}})$	$1.00077 + i\,7.05 \times 10^{-3}$
$\cos(\theta_{p,\mathrm{ET}})$	$-7.97 \times 10^{-2} + i\,8.85 \times 10^{-2}$

$$\cos(\theta_b) = \sqrt{\frac{(k_1/k_0)^2 - 1}{(\rho_1/\rho_0)^2 - 1}}, \quad \Im(\cos(\theta_b)) < 0. \tag{48}$$

With this choice for $\Im(\cos(\theta_b))$, $\Re(\cos(\theta_b))$ is positive. An iterative method with the CM model can be used to obtain the modified Brewster angle. Predictions with the CM, the BTHT and ET models and the nonmodified cosine and sine of the Brewster angle are given in Table II. In the complex sin (θ) plane, the nonmodified sin (θ_b) is closer to the real axis. This can explain why the predicted variation of $|R|$ around the minimum is faster than with the other models.

For a thin porous layer of constant thickness, the reflection coefficient has a pole at an angle of incidence θ_p close to $\pi/2$ which can be linked to a surface wave.[16] The angle θ_p is characterized by

$$\Re(\cos(\theta_p)) < 0, \qquad \Im(\cos(\theta_p)) > 0. \tag{49}$$

Then the incident wave must be selected from

$$\Re(k_{z,n+1,0}) < 0 \quad \text{or} \quad \Im(k_{z,n+1,0}) > 0. \tag{50}$$

An iterative method can be used to obtain cos (θ_p), satisfying the same conditions for corrugations over a rigid impervious backing. An angle of incidence satisfying these conditions has been found with the different methods. Predictions are given in Table III for the different methods. All methods give similar results, with a sin (θ_p) further from the real axis than the one obtained for the porous medium with constant thickness. Many other comparisons, not reported here, between the complex reflection coefficients predicted with the FEM and the CM methods, have been performed for different shapes of corrugations and layers with different constant thicknesses between the corrugations and the rigid impervious layer.

VI. CONCLUSION

Reflection coefficients at oblique incidence with underlying rigid impervious surfaces or semi-infinite porous layers with 2D semi-circular porous corrugations have been predicted with a new CM model and a finite-element model. The distance between the corrugations is smaller than the wavelength in air and only one mode is propagative. A reflection coefficient can be evaluated from the ratio of the reflected and incident propagative modes. The finite-element model and the CM model always give very similar results. Other comparisons are performed with the CM model and previous

models including the BTHT model and the ET model. Good agreement exists between the CM model and the ET model when the overlying surface is a rigid impervious surface. In this case, the ET model and the initial Twersky model are identical. In the other cases, there is a non-negligible difference between the predictions of the previous models and the CM model. The largest discrepancy appears at small angles of incidence for the corrugated porous medium. This could be due to the strong difference at these angles of incidence between the BTHT model and the initial Tolstoy model. The difference is also noticeable for the Brewster angle related to a corrugated semi-infinite porous layer. However, the predicted locations of the pole of the reflection coefficient when the underlying surface is a rigid and impervious surface are close to each other in the complex sin (θ) plane.

APPENDIX A: DETAILS ON THE DERIVATION OF THE DISPERSION RELATION

The subscripts j,l are removed for A_i, B_i, α, and β.
The Floquet condition gives the expression of A_3 and B_3

$$B_3 = B_1 e^{iD(\alpha - k_x)}, \tag{A1}$$

$$A_3 = A_1 e^{-iD(\alpha + k_x)}. \tag{A2}$$

At the vertical plane surfaces between the air and porous medium, continuity and displacement conditions are verified. With the preceding relation, this leads to the four following relations linking A_1, B_1, A_2, and B_2:

$$A_1\left[1-\frac{\rho_1\alpha}{\rho_0\beta}\right]e^{-i(\alpha+\beta)[D/2-d_j]}+B_1\left[1+\frac{\rho_1\alpha}{\rho_0\beta}\right]e^{i(\alpha-\beta)[D/2-d_j]}=2B_2, \tag{A3a}$$

$$A_1\left[1+\frac{\rho_1\alpha}{\rho_0\beta}\right]e^{-i(\alpha-\beta)[D/2-d_j]}+B_1\left[1-\frac{\rho_1\alpha}{\rho_0\beta}\right]e^{i(\alpha+\beta)[D/2-d_j]}=2A_2, \tag{A3b}$$

$$A_2\left[1-\frac{\rho_0\beta}{\rho_1\alpha}\right]e^{-i(\alpha+\beta)[-D/2+d_j]}+B_2\left[1+\frac{\rho_0\beta}{\rho_1\alpha}\right]e^{-i(\alpha-\beta)[-D/2+d_j]} = 2B_1e^{iD(\alpha-k_x)}, \tag{A3c}$$

$$A_2\left[1+\frac{\rho_0\beta}{\rho_1\alpha}\right]e^{i(\alpha-\beta)[-D/2+d_j]}+B_2\left[1-\frac{\rho_0\beta}{\rho_1\alpha}\right]e^{i(\alpha+\beta)[-D/2+d_j]} = 2A_1e^{-iD(\alpha+k_x)}. \tag{A3d}$$

Algebraic manipulations allow to eliminate A_2 and B_2

$$A_1\left[1+\frac{\rho_1\alpha}{\rho_0\beta}\right]\left[1-\frac{\rho_0\beta}{\rho_1\alpha}\right]e^{i\beta(D-2d_j)}+B_1\left[1-\frac{\rho_1\alpha}{\rho_0\beta}\right]\left[1-\frac{\rho_0\beta}{\rho_1\alpha}\right]e^{i(\alpha+\beta)(D-2d_j)}+A_1\left[1-\frac{\rho_1\alpha}{\rho_0\beta}\right]\left[1+\frac{\rho_0\beta}{\rho_1\alpha}\right]e^{-i\beta(D-2d_j)} + B_1\left[1+\frac{\rho_1\alpha}{\rho_0\beta}\right]\left[1+\frac{\rho_0\beta}{\rho_1\alpha}\right]e^{i(\alpha-\beta)(D-2d_j)} = 4B_1e^{iD(\alpha-k_x)},$$

$$A_1\left[1+\frac{\rho_1\alpha}{\rho_0\beta}\right]\left[1+\frac{\rho_0\beta}{\rho_1\alpha}\right]e^{-i(\alpha-\beta)(D-2d_j)}+B_1\left[1-\frac{\rho_1\alpha}{\rho_0\beta}\right]\left[1+\frac{\rho_0\beta}{\rho_1\alpha}\right]e^{i\beta(D-2d_j)}+A_1\left[1-\frac{\rho_1\alpha}{\rho_0\beta}\right]\left[1-\frac{\rho_0\beta}{\rho_1\alpha}\right]e^{-i(\alpha+\beta)(D-2d_j)} + B_1\left[1+\frac{\rho_1\alpha}{\rho_0\beta}\right]\left[1-\frac{\rho_0\beta}{\rho_1\alpha}\right]e^{-i\beta(D-2d_j)} = 4A_1e^{-iD(\alpha+k_x)}.$$

These last two equations correspond to a homogeneous linear system whose determinant Δ is equal to zero

$$\Delta = -8e^{-ik_xD}w(\alpha,\beta), \tag{A4}$$

$$w(\alpha,\beta) = 4\cos(k_xD)-\cos(\beta(D-2d_j)+2\alpha d_j)\left(1+\frac{\alpha\rho_1}{\beta\rho_0}\right)\times\left(1+\frac{\beta\rho_0}{\alpha\rho_1}\right)+\cos(\beta(D-2d_j)-2\alpha d_j)\times\left(1-\frac{\alpha\rho_1}{\beta\rho_0}\right)\left(1-\frac{\beta\rho_0}{\alpha\rho_1}\right).$$

APPENDIX B: PROOF OF THE ORTHOGONALITY RELATION (24)

Layer j is considered. Let $\Omega = \left[-\frac{D}{2};\frac{D}{2}\right]$ be divided into three subdomains Ω_i $(i=1,2,3)$ on which the properties of the medium are constant. Density $\rho_j(x)$ is denoted by ρ_i on each one of these subdomains. Note that $\rho_i(x)$ is not supposed to be real.

Let l and m be in $\mathbb{Z}$ so that $l \neq m$ (and then $\alpha_{j,m} \neq \alpha_{j,l}$). The x-dependences associated with modes m and l have the following properties (here given for mode m):

(1) Eigenfunctions of $\mathcal{L}_j$:

$$\mathcal{L}_j\, p_{j,m} = -\alpha_{j,m}^2\, p_{j,m}. \tag{B1}$$

(2) Continuity of displacement and pressure: $p_{j,m}(x)$ and $\frac{p'_{j,m}(x)}{\rho_j(x)}$ are continuous functions.

(3) Floquet condition of periodicity

$$p_{j,m}\left(\frac{D}{2}\right) = \delta\cdot p_{j,m}\left(-\frac{D}{2}\right),$$
$$\frac{p'_{j,m}}{\rho_j}\left(\frac{D}{2}\right) = \delta\cdot\frac{p'_{j,m}}{\rho_j}\left(-\frac{D}{2}\right), \quad \delta = e^{jk_xD}. \tag{B2}$$

Density $\rho_j(x)$ is a complex step-wize constant function on Ω. It is then straightforward to prove that

$$\mathcal{L}\left[\frac{p_{j,m}()}{\rho_j(x)}\right] = -\alpha_{j,m}^2\left[\frac{p_{j,m}(x)}{\rho_j(x)}\right] \text{for almost all } x. \tag{B3}$$

This relation is multiplied by $p_{j,l}(-x)$ and integrated over Ω.

$$\int_\Omega \mathcal{L}\left[\frac{p_{j,m}(x)}{\rho_j(x)}\right] p_{j,l}(-x)\mathrm{d}x = -\alpha_{j,m}^2 \int_\Omega \left[\frac{p_{j,m}(x)}{\rho_j(x)}\right] p_{j,l}(-x)\mathrm{d}x. \tag{B4}$$

The left hand side is the sum of the three $I_i(m,l)$ integrals on Ω_i

$$\begin{aligned} I_i(m,l) &= \int_{\Omega_i} \mathcal{L}\left[\frac{p_{j,m}(x)}{\rho_i}\right] p_{j,l}(-x)\,\mathrm{d}x, = \int_{\Omega_i}\left(-\frac{p\prime\prime_{j,m}(x)}{\rho_i} + (k_0^2 - k_j^2(x))\frac{p_{j,m}(x)}{\rho_i}\right) p_{j,l}(-x)\,\mathrm{d}x, \\ &= -\left[\frac{p\prime_{j,m}(x)p_{j,l}(-x)}{\rho_i}\right]_{\Omega_i} + \int_{\Omega_i} \frac{p\prime_{j,m}(x)p\prime_{j,l}(-x)}{\rho_i} + (k_0^2 - k_j^2(x))\frac{p_{j,m}(x)p_{j,l}(-x)}{\rho_i}\,\mathrm{d}x. \end{aligned}$$

Due to the pressure and displacement continuities and the Floquet condition, one has

$$\begin{aligned} &\sum_{i=1}^{3}\left[\frac{p\prime_{j,m}(x)}{\rho_i} p_{j,l}(-x)\right]_{\Omega_i} \\ &\quad = \frac{p\prime_{j,m}\left(\frac{D}{2}\right)}{\rho\left(\frac{D}{2}\right)} p_{j,l}\left(-\frac{D}{2}\right) - \frac{p\prime_{j,m}\left(-\frac{D}{2}\right)}{\rho\left(-\frac{D}{2}\right)} p_{j,l}\left(\frac{D}{2}\right) = 0. \end{aligned} \tag{B5}$$

Relation (B4) then reads

$$\begin{aligned} &\int_\Omega \frac{p\prime_{j,m}(x)p\prime_{j,l}(-x)}{\rho_j(x)} + (k_0^2 - k_j^2(x))\frac{p_{j,m}(x)p_{j,l}(-x)}{\rho_j(x)}\,\mathrm{d}x \\ &\quad = -\alpha_{j,m}^2 \int_\Omega \frac{p_{j,m}(x)p_{j,l}(-x)}{\rho_j(x)}\mathrm{d}x. \end{aligned} \tag{B6}$$

A similar relation can be obtained by inverting l and m

$$\int_\Omega \frac{p\prime_{j,l}(x)p\prime_{j,m}(-x)}{\rho_j(x)} + (k_0^2 - k_j^2(x))\frac{p_{j,l}(x)p_{j,m}(-x)}{\rho_j(x)}\,\mathrm{d}x$$

$$= -\alpha_{j,l}^2 \int_\Omega \frac{p_{j,l}(x)p_{j,m}(-x)}{\rho_j(x)}\mathrm{d}x. \tag{B7}$$

The left hand sides of the the last two equations are equal due to the symmetry of Ω, $\rho_j(x)$, and $k_j(x)$. The orthogonality property is then finally obtained by subtracting these two equations ($\alpha_{j,m} = \alpha_{j,l}$).

APPENDIX C: ITERATIVE METHOD

The quantity $w(\beta)$ given by Eq. (22) initially equal to 0 in the elementary volume j must be set equal to 0 in the elementary volume $j+1$. At each step of the iterations the wave-number component β is replaced by $\beta + \Delta\beta$ where $\Delta\beta$ is given by

$$\Delta\beta = -\frac{w\prime(\beta)}{2w(\beta)}. \tag{C1}$$

The derivative $w'(\beta)$ is given by

$$\begin{aligned} w\prime(\beta) &= \sin[\beta(D-2d)+2\alpha d]\left(1+\frac{\alpha\rho_1}{\beta\rho_0}\right)\left(1+\frac{\beta\rho_0}{\alpha\rho_1}\right)\left(D-2d+\frac{2\beta d}{\alpha}\right) \\ &\quad - \cos[\beta(D-2d)+2\alpha d]\left[\frac{\rho_0}{\alpha\rho_1}\left(1-\frac{\beta^2}{\alpha^2}\right)\left(1+\frac{\alpha\rho_1}{\beta\rho_0}\right)+\frac{\rho_1}{\alpha\rho_0}\left(1-\frac{\alpha^2}{\beta^2}\right)\left(1+\frac{\beta\rho_0}{\alpha\rho_1}\right)\right] \\ &\quad + \sin[\beta(D-2d)-2\alpha d]\left(1-\frac{\alpha\rho_1}{\beta\rho_0}\right)\left(1-\frac{\beta\rho_0}{\alpha\rho_1}\right)\left(D-2d-\frac{2\beta d}{\alpha}\right) \\ &\quad - \cos[\beta(D-2d)-2\alpha d]\left[-\frac{\rho_0}{\alpha\rho_1}\left(1-\frac{\beta^2}{\alpha^2}\right)\left(1-\frac{\alpha\rho_1}{\beta\rho_0}\right)-\frac{\rho_1}{\alpha\rho_0}\left(1-\frac{\alpha^2}{\beta^2}\right)\left(1-\frac{\beta\rho_0}{\alpha\rho_1}\right)\right]. \end{aligned} \tag{C2}$$

An indirect test for the evaluation of β is obtained by checking the orthogonality of the different modes for the related elementary volume.

[1]K. Attenborough and S. Taherzadeh, "Propagation from a point source over a rough finite impedance boundary," J. Acoust. Soc. Am. **98**, 1717–1722 (1995).

[2]I. Tolstoy, "Coherent sound scatter from a rough interface between arbitrary fluids with particular reference to roughness element shapes and corrugated surfaces," J. Acoust. Soc. Am. **75**, 1–22 (1984).

[3]R.-J. Lucas and V. Twersky, "Coherent response to a point source irradiating a rough plane," J. Acoust. Soc. Am. **76**, 1847–1863 (1984).

[4]P. Boulanger, K. Attenborough, and Q. Quin, "Effective impedance of surfaces with porous roughness: Models and data," J. Acoust. Soc. Am. **103**, 1146–1156 (2005).

[5]V. Twersky, "Reflection and scattering of sound by correlated rough surfaces," J. Acoust. Soc. Am. **73**, 85–94 (1983).
[6]V. Easwaran and M.-L. Munjal, "Finite element analysis of wedges used in anechoic chambers," J. Sound Vib. **160**, 333–350 (1993).
[7]T. Kar and M.-L. Munjal, "Plane wave analysis of acoustic wedges using the boundary condition transfer algorithm," Appl. Acoust. **67**, 901–917 (2006).
[8]Y. Kang and J. Bolton, "Sound transmission, through elastic porous wedges and foam layers having spatially graded properties," J. Acoust. Soc. Am. **102**, 3319–3332 (1997).
[9]S. Schneider, "Experimental and numerical investigations on a melamine wedge," J. Acoust. Soc. Am. **124**, 1568–1576 (2008).
[10]X. Olny and C. Boutin, "Acoustic wave propagation in double porosity media," J. Acoust. Soc. Am. **114**, 73–89 (2003).
[11]F.-X. Bécot, L. Jaouen, and E. Gourdon, "Application of the dual porosity theory to irregularly shaped porous materials," J. Acoust. Soc. Am. **129**, 3, 715–724 (2011).
[12]R.-B. Evans, "A coupled mode solution for acoustic propagation in a waveguide with stepwise depth variation of a penetrable bottom," J. Acoust. Soc. Am. **74**, 188–195 (1983).
[13]V. Pagneux, N. Amir, and J. Kergomard, "A study of wave propagating in varying cross-section waveguides by modal decomposition. Part I. Theory and validation," J. Acoust. Soc. Am. **100**, 2034–2048 (1996).
[14]D. Johnson, J. Koplik, and R. Dashen, "Theory of dynamic permeability and tortuosity in fluid-saturated porous media," J. Fluid Mech. **176**, 379–402 (1987).
[15]Y. Champoux and J. Allard, "Dynamic tortuosity and bulk modulus in air-saturated porous media," J. Appl. Phys. **70**, 1975–1979 (1991).
[16]J.-F. Allard and N. Atalla, *Propagation of Sound in Porous Media-Modelling Sound Absorbing Materials* (Wiley, New York, 2009), Chap. V, p. 84 and Chap. VII, pp 146–148.
[17]O. Dazel, B. Brouard, C. Depollier, and S. Griffiths, "An alternative Biot's displacement formulation for porous materials," J. Acoust. Soc. Am. **121**, 3509–3516 (2007).
[18]H. Lamb, *Hydrodynamics* (Dover, New York, 1945), Chap. IV, p. 85.
[19]C. Hickey, D. Leary, J.-F. Allard, and M. Henry, "Impedance and Brewster angle measurement for thick porous layers," J. Acoust. Soc. Am. **118**, 1503–1509 (2005).